

# In Situ Performance Monitoring of Electrochemical Oxygen and Hydrogen Peroxide Sensors in an Additively Manufactured Modular Microreactor

Moritz Doering, Laura L. Trinkies, Jochen Kieninger, Manfred Kraut, Stefan J. Rupitsch, Roland Dittmeyer, Gerald A. Urban, and Andreas Weltin\*



Cite This: *ACS Omega* 2024, 9, 19700–19711



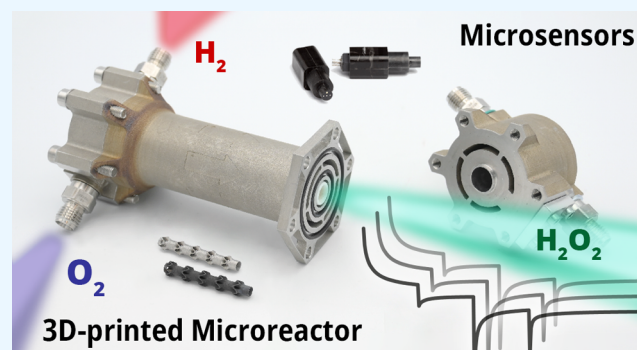
Read Online

ACCESS |

Metrics & More

Article Recommendations

**ABSTRACT:** Miniaturized and microstructured reactors in process engineering are essential for a more decentralized, flexible, sustainable, and resilient chemical production. Modern, additive manufacturing methods for metals enable complex reactor-geometries, increased functionality, and faster design iterations, a clear advantage over classical subtractive machining and polymer-based approaches. Integrated microsensors allow online, in situ process monitoring to optimize processes like the direct synthesis of hydrogen peroxide. We developed a modular tube-in-tube membrane reactor fabricated from stainless steel via 3D printing by laser powder bed fusion of metals (PBF-LB/M). The reactor concept enables the spatially separated dosage and resaturation of two gaseous reactants across a membrane into a liquid process medium. Uniquely, we integrated platinum-based electrochemical sensors for the online detection of analytes to reveal the dynamics inside the reactor. An advanced chronoamperometric protocol combined the simultaneous concentration measurement of hydrogen peroxide and oxygen with monitoring of the sensor performance and self-calibration in long-term use. We demonstrated the highly linear and sensitive monitoring of hydrogen peroxide and dissolved oxygen entering the liquid phase through the membrane. Our measurements delivered important real-time insights into the dynamics of the concentrations in the reactor, highlighting the power of electrochemical sensors applied in process engineering. We demonstrated the stable continuous measurement over 1 week and estimated the sensor lifetime for months in the acidic process medium. Our approach combines electrochemical sensors for process monitoring with advanced, additively manufactured stainless steel membrane microreactors, supporting the power of sensor-equipped microreactors as contributors to the paradigm change in process engineering and toward a greener chemistry.



and oxygen ( $O_2$ ) on noble metal catalysts.<sup>4,5</sup> In recent years, another fascinating research field arose from the idea to utilize electrochemical reduction as a fabrication route for hydrogen peroxide. Investigations were realized to enable the production of  $H_2O_2$  via the two-electron reduction of oxygen. This approach as well uses microreactors in a decentralized manner and the increase in sustainability is comparably promising as it can be conducted in water or aqueous solutions and does not produce any waste.<sup>6–8</sup>

## 1. INTRODUCTION

In recent years, flow chemistry using microreactors has become a promising alternative to established batch processes in large plants. Monbaliu et al. underlined the importance of microreactors as a contribution toward next generation process engineering, calling miniaturized flow reactors a new paradigm.<sup>1</sup> Microreactors are gaining importance in different fields of application. Based on their improved capability for upscaling with regard to production volume by combining several reactor modules, a flow-chemistry-approach is beneficial in the different stages of testing and producing fine chemicals like drug substances.<sup>2</sup> Due to their advantage of enhanced heat transfer, microreactors facilitate, e.g., exothermic organometallic reactions in organic chemistry.<sup>3</sup> In process engineering, lowering the dimensions of reaction chambers to microchannels allows the safe operation of catalytic reactions that bear explosion risk at larger volumes, like the direct synthesis of hydrogen peroxide ( $H_2O_2$ ) from hydrogen ( $H_2$ )

and oxygen ( $O_2$ ) on noble metal catalysts.<sup>4,5</sup> In recent years, another fascinating research field arose from the idea to utilize electrochemical reduction as a fabrication route for hydrogen peroxide. Investigations were realized to enable the production of  $H_2O_2$  via the two-electron reduction of oxygen. This approach as well uses microreactors in a decentralized manner and the increase in sustainability is comparably promising as it can be conducted in water or aqueous solutions and does not produce any waste.<sup>6–8</sup>

**Received:** March 6, 2024  
**Revised:** March 21, 2024  
**Accepted:** March 27, 2024  
**Published:** April 16, 2024



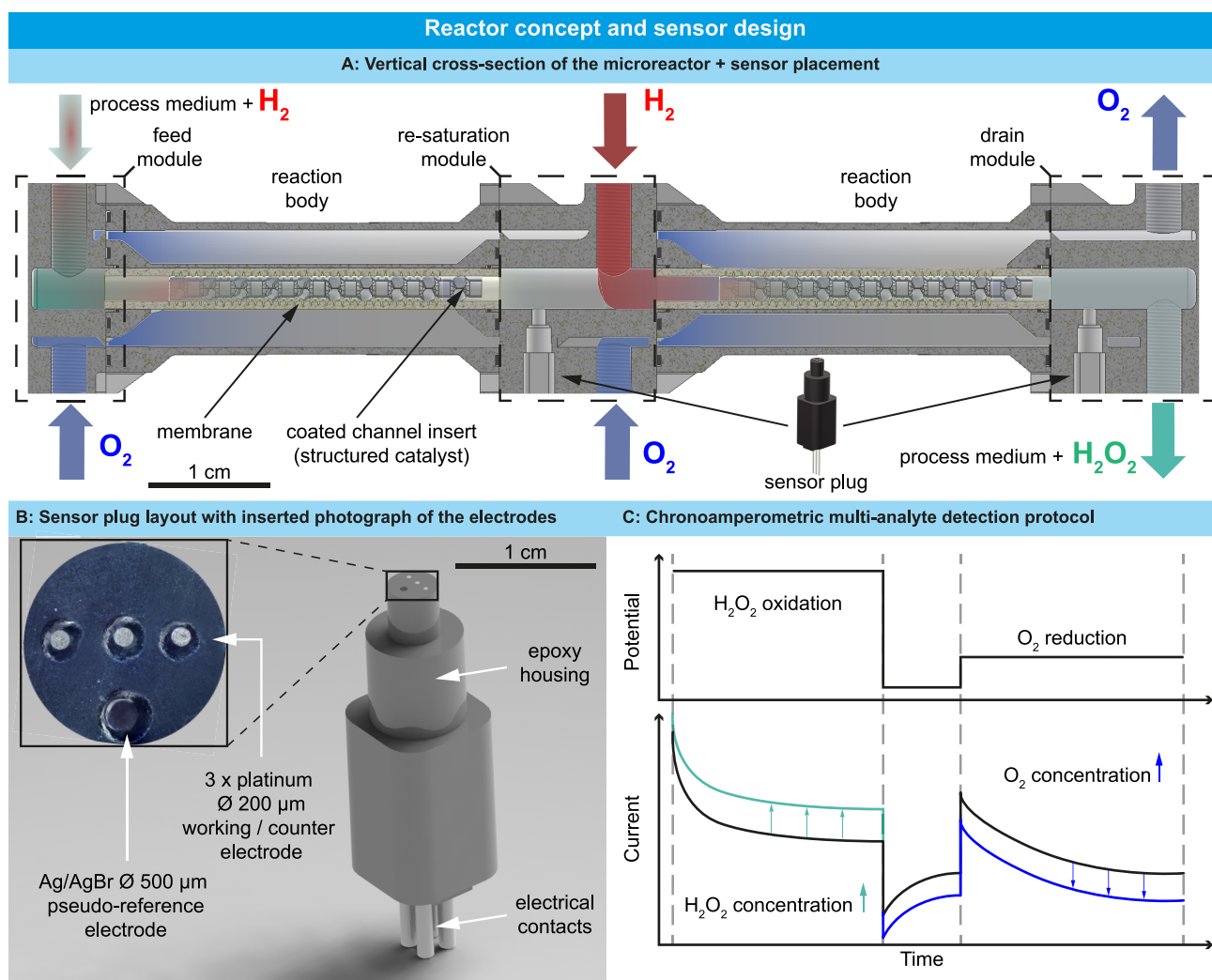


**Figure 1.** Concept of the sensor-equipped, additively manufactured reactor for the direct synthesis of hydrogen peroxide. (A) Cross section along the reactor length, indicating the in- and outlets of the process media and gases as well as the position of the electrochemical sensors. (B) Sensor plug for insertion into the reaction channel with an inserted photograph of the electrode plane. (C) Illustration of the used chronoamperometric measurement protocol for the quantification of hydrogen peroxide and dissolved oxygen.

Classically, microreactors are fabricated with techniques optimized for 2-dimensional patterning.<sup>9</sup> Nowadays, additive manufacturing is superior to traditional manufacturing with respect to the unit costs, if the production volume is low, or the product complexity is high.<sup>10</sup> Furthermore, with additive manufacturing, the realization of complex geometries, including for example internal cavities, is possible.<sup>11</sup> All of these aspects are beneficial for advanced microreactors, making additive manufacturing a highly promising fabrication method. Stainless steel is a very suitable material for microreactors used to synthesize  $\text{H}_2\text{O}_2$  because it is highly pressure-resistant, usable at low pH and has a high thermal conductivity. A variety of techniques for the additive manufacturing of metals has been under investigation lately and is already applied.<sup>10,12,13</sup> The microreactor demonstrated in this work was fabricated using the laser powder bed fusion of metals (PBF-LB/M).

In order to control and optimize both types of decentralized production, the direct synthesis of  $\text{H}_2\text{O}_2$ , and the electro-synthesis of hydrogen peroxide in microreactors, a real-time measurement of reactant concentrations like dissolved  $\text{O}_2$ , as well as the synthesized  $\text{H}_2\text{O}_2$ , is essential. Electrochemical sensors are highly suitable for this purpose due to their defined

zero-point, high temporal resolution, high sensitivity over a wide range of analyte concentrations, and the possibility to miniaturize them.<sup>14–16</sup>

In general,  $\text{H}_2\text{O}_2$  and the dissolved gases  $\text{H}_2$  and  $\text{O}_2$  in the liquid phase can be detected by various approaches, with electrochemical and optical sensors being the most common for real-time in situ monitoring.<sup>17,18</sup> Electrochemical sensors are typically based on the conversion of the analytes at a noble metal electrode, often covered with a suitable membrane.<sup>19</sup> Miniaturized optical sensors, e.g., based on luminescence,<sup>20,21</sup> fluorescence,<sup>22</sup> or absorption<sup>23</sup> spectroscopic/spectrophotometric techniques, often consist of an optical fiber or sensor patch coated with an appropriate indicator dye.<sup>17</sup> Fiber-optical in line oxygen sensors in custom 3D-printed stainless steel flow reactors have been demonstrated at a pressure of 7 bar and up to 42 mM oxygen in the presence of organic solvents.<sup>24</sup> Optical at-line sensors for  $\text{H}_2\text{O}_2$  up to 200  $\mu\text{M}$  have recently been shown.<sup>25</sup>

Rugged sensor probes for industrial applications based on either principle, such as commonly found in bioprocess monitoring, are typically centimeter-scale rod-shaped devices with millimeter-size sensor elements at the tip or patches

which require optical access. These are challenging to integrate in microreactors, especially highly customized steel reactors, due to limitations in geometry, a potential lack of optical access, the required resistance to harsh environments and high pressures, and also cost if multiple sensors are required to map the reactor along its length or width. Chip-based sensors with microelectrode arrays promise high spatial resolution but are also difficult to integrate into stainless steel reactors due to the challenges in interfacing and lack of robustness. Besides these limitations, in processes such as  $\text{H}_2\text{O}_2$  synthesis, offline methods such as titration<sup>26</sup> or ultraviolet/visible/near-infrared spectroscopy<sup>27,28</sup> are still commonly employed to detect the analyte, often outside or downstream of the reactor.

Besides their promising analytical performance for monitoring the reaction, miniaturized, robust electrochemical sensors allow integration into stainless steel microreactors without lowering the pressure-resistance of the system or interfering with the synthesis reaction. Electrochemical microsensors enable the continuous, marker-free, online concentration measurement in direct contact with the process medium. Specifically, Pt electrodes are capable of detecting and quantifying  $\text{H}_2$ ,  $\text{O}_2$ , and  $\text{H}_2\text{O}_2$  simultaneously, by the application of advanced chronoamperometric protocols.<sup>29</sup> These protocols can also be used for self-calibration during long-term use in harsh environments.

In this work, we present a sensor-equipped, additively manufactured stainless steel microreactor for the direct synthesis of  $\text{H}_2\text{O}_2$ . We discuss the concept and requirements for the additive manufacturing process by PBF-LB/M of stainless steel. A planar design was successfully transferred to a tube-in-tube concept using the advantages of modern 3D-printing techniques, which allowed a modular concept for the membrane microreactor with integrated electrochemical sensors. The fabrication process and leakage-free performance of the reactor components was qualified. Finally, the in situ process monitoring of  $\text{H}_2\text{O}_2$  and  $\text{O}_2$  was demonstrated using electrochemical sensors, and sensor performance and long-term stability in process media were evaluated. Sensor-equipped, 3D-printed reactors for flow chemistry can promote more efficient, automated as well as safer process engineering and facilitate the transition to green chemistry.

## 2. MICROREACTOR DEVELOPMENT: CONCEPT AND REQUIREMENTS

Microreactors for  $\text{H}_2\text{O}_2$  direct synthesis, a multiphase reaction, require two independent, spatially separated gas inlets, a membrane to enable dissolution of the gases in the process medium, and a liquid channel, including the catalyst, for the reaction and product collection. Previous planar designs were fabricated by subtractive machining using CNC-milling of stainless steel plates.<sup>29–32</sup> Catalysts were integrated, e.g., in suspension or as a fixed bed.<sup>30,32</sup> Additive manufacturing methods allow the transfer to more complex geometries such as tube-in-tube structures (Figure 1A), enabling a more modular concept, among other advantages.

For the development of an additively manufacturable reactor design, there are requirements from the point of fabrication, chemical reaction, and process environment.

**2.1. Fabrication Requirements.** To be suitable for modifications to variable operating conditions at the development stage and for individual changes for later use, the designed reactor has to be adaptive and modular by its design. The manufacturing of components via additive

manufacturing does not only allow more complex geometries, it is also cheaper for smaller batches.<sup>33,34</sup>

For the practical realization of the design of the reactor in this study, additive manufacturing was therefore chosen as fabrication method. Although the production of components by means of additive manufacturing allows a high degree of flexibility in design, some design guidelines must also be observed in additive manufacturing at the same time. These guidelines usually depend on the 3D-printing method. The restrictions given in the following arise from the chosen additive manufacturing process, the laser powder bed fusion of metals method (PBF-LB/M), and the used printer, a Realizer 125 system (DMG Mori, Bielefeld, Germany). In designs for PBF-LB/M, overhangs in the component geometry are to be avoided as insufficient heat dissipation would be the consequence and overhangs realized by the usage of support structures would lead to additional postfabrication steps.<sup>35–39</sup>

Due to thermal effects, large, planar, thin walls must be bypassed in the geometry design<sup>40,41</sup> to prevent deformation due to residual stress.<sup>42</sup> Further care must be taken to keep the component volume as small as possible because the manufacturing costs incurred in additive manufacturing using PBF-LB/M are directly proportional to its material volume and especially to the component height. Since not all available materials are suitable for PBF-LB/M processes, the material selection is determined not only by the chemical inertness, but also by the applicability in the selected manufacturing process.<sup>42</sup> The printer used for the manufacturing of the parts in this work has a nominal build volume of  $125 \times 125 \times 200 \text{ mm}^3$ . That results in a maximum build height of 190 mm for the reactor. This derived maximum build height is based on experience, as the height of the build platform must also be considered in the design and subtracted from the nominal build height.

**2.2. Reaction Requirements.** For the direct synthesis reaction of  $\text{H}_2\text{O}_2$ , the reactants  $\text{H}_2$  and  $\text{O}_2$  must be safely brought into contact at a noble metal catalyst. To prevent the formation of an explosive atmosphere, spatial separation of the feed of  $\text{H}_2$  and  $\text{O}_2$  gases must be considered during the development of the design. It is important to ensure tight sealing of the reaction chamber filled with the liquid reaction medium as well as sealing of the gas-supplying volume to the outside to prevent the reactants from leaking into the environment. The material used to manufacture the reactor and, above all, the components in contact with the medium must be chemically inert to avoid any undesirable effect on the reaction. At the same time, the components must have sufficient pressure resistance to allow increased operating pressures, if necessary, and thus higher reactant quantities in the reaction solution. The reaction takes place in the liquid phase, but the catalyst is present as a solid. For this reason, a way must be found to integrate the catalyst into the reactor without requiring a consecutive filtrative separation step.

**2.3. Process Requirements.** Continuous flow processes allow for easy automation as well as good reproducibility and process reliability.<sup>43</sup> For these reasons, the reactor concept to be developed should be adapted to this type of process operation. For the connection of the reactor to the plant periphery, appropriate connecting pieces and contact surfaces of the connecting screw heads must be considered in the design. Attention must be paid to the modularity of the individual components. To monitor the process in situ and during the operation of the plant, sensor inlets for

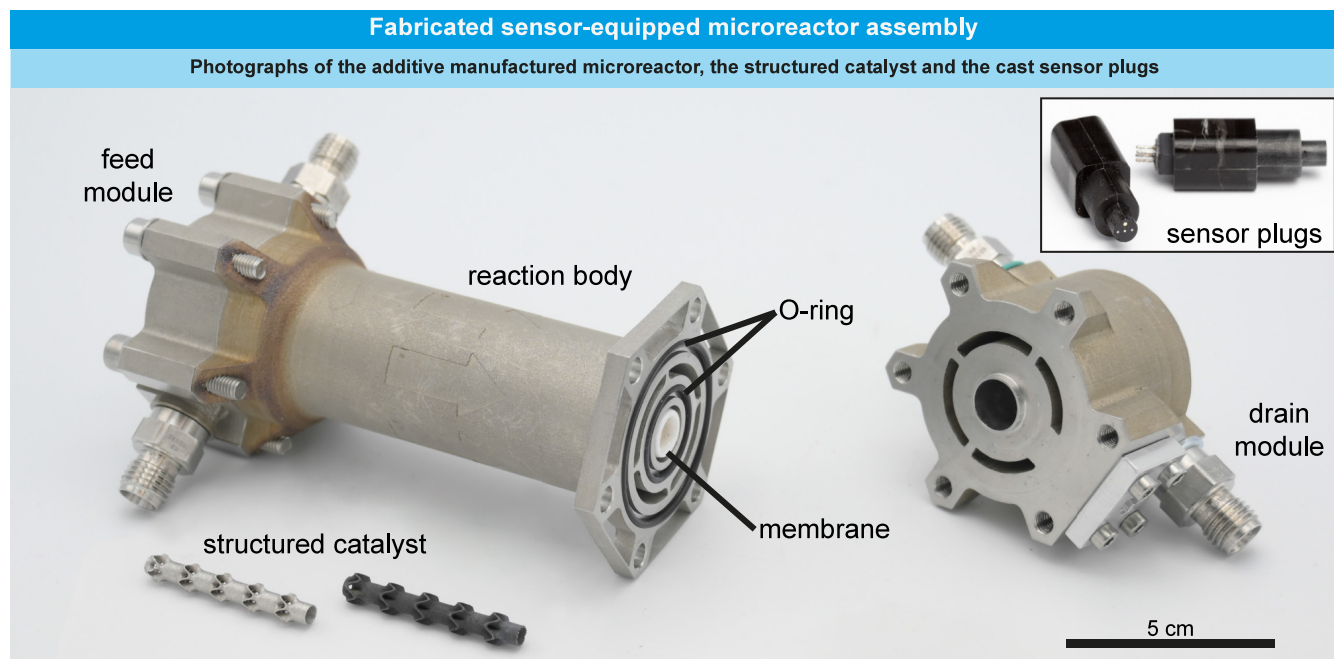


**Figure 2.** Photograph of the additively manufactured stainless steel microreactor with inserted tubular membrane, 3D-printed structured catalysts, and cast sensor plugs.

corresponding sensor plugs (Figure 1B) that detect the analytes using a chronoamperometric sensor protocol (Figure 1C) have to be integrated.

**2.4. Deduced Reactor Design.** From the requirements, we deduced the reactor design shown in Figure 1A, combining the design rules of the fabrication method with the requirements of the application. The cross-section shows the tube-in-tube design with the process medium in the inner tube, the gas compartments in the outer tube, and the membrane in between. The structured catalysts, acting also as fluid guiding elements,<sup>44</sup> are placed in the inner tube within the process medium. The modular concept consists of feed module, reaction body, and drain module (Figure 2). A resaturation module connects two reaction bodies. Each resaturation/drain module has an opening for placing an electrochemical sensor. Hydrogen gas can be presaturated in the process medium, whereas O<sub>2</sub> is supplied through the membrane, and hydrogen can also be resaturated directly into the liquid phase (Figure 1A). All metallic components are 3D-printed in stainless steel via a PBF-LB/M process.

Classically, wall coatings can be used for integrating solid catalysts into a reactor without the necessity for consecutive filtration steps. However, it is difficult to replace the catalyst in this case without replacing the entire reactor module as it might be needed, e.g., after deactivation of the catalyst. As a solution, structured catalysts were chosen for the integration of the solid catalyst in our concept<sup>45,46</sup> (Figures 1A and 2). To ensure the safety of the process when contacting the reactants, membrane reactors in a distributor configuration are considered, which allow the selective supply of gaseous substances.<sup>47</sup> Tubular membrane distributors can be used in simple setups, e.g., via adapted tube-in-tube reactors with O<sub>2</sub>-permeable<sup>48</sup> tubes made from fluorinated polymer.<sup>49,50</sup> To fulfill the process requirements of synthesis reactions, the membrane consisting of a hydrophobic PDMS layer on a tubular ceramic support was integrated into an additively manufacturable design oriented to conventional catalytic

membrane reactors.<sup>51</sup> Small dimensions of the reaction chamber can be used not only to ensure that small reaction volumes are present in the system, but also to ensure that the critical length, which would be required for an explosion to proceed in the event of an accident, is exceeded.<sup>52</sup> Further, this miniaturization allows for a compact reactor and thus a small physical footprint. As is required for additively manufactured reactors,<sup>53</sup> overhangs were avoided by appropriate bevels, for example, on the flanges connecting the individual modules.

Via the tubular ceramic membrane with active PDMS coating enclosing the tubular channel, the O<sub>2</sub> guided in the outer gas feed channel can be fed to the reaction medium in a controlled and bubble-free manner. In this concept, the synthesis reaction occurs at the surface of the structured catalyst. The concentrations of the reactants and the product in the reaction medium can be monitored via insertable electrochemical sensors directly downstream of the reaction chamber. In later operation, there is the possibility of postsaturation via the postsaturation module if the necessity is detected via the sensors. Both O<sub>2</sub> and H<sub>2</sub> can be supplied to the system via resaturation points, if required (Figure 1A). The arrangement of the inlet and outlet points for liquid and gases are each chosen to allow the liquid to flow in and out of the reaction volume supported by gravity, while avoiding intrusion into the H<sub>2</sub> postsaturation channel. The sensor measurement points are each placed along the flow direction upstream of the postsaturation points to prevent one or more sensor electrodes from being covered by individual gas bubbles from the resaturating gas stream and thus prevent sensor failure. The product leaves the reactor as a component that is dissolved in the reaction medium via an outlet on the underside of the drain module. Due to the modular design, a membrane reactor cascade can be derived by joining several reactor modules. Lateral leakage of the gases from the membrane at the head ends was prevented by the manufacturer by sealing the ends with glass. This part was radially separated from the external gas supply channel by enclosing the O-rings. The seal between

the reaction channel and the reactant feed channel as well as the seal of the reactant feed channel to the environment was realized via O-ring-groove pairings (Figure 2). To minimize the postprocessing steps after additive manufacturing, the necessary threads for subsequent assembly were already printed (Figure 2). Only the necessary sealing surfaces and associated O-ring grooves and fits had to be reworked after printing to ensure the necessary surface quality. The sensor openings were prepared in the same way and postmachined in order to further reduce gas or liquid leaking by means of high surface qualities. The sensors were fixed in the module via a separate adapting plate (Figure 2).

### 3. ELECTROCHEMICAL SENSORS AND METHODS

**3.1. Process Media.** A 0.15 mM sulfuric acid (pH = 3.5) was diluted from a 0.5 M sulfuric acid stock solution (VWR Chemicals, France) with deionized water. Halides such as NaBr may serve as inhibitors for the side reactions of direct synthesis.<sup>54</sup> Thus, sodium bromide ( $\geq 99\%$ , Sigma-Aldrich, USA) was added in the majority of the experiments, resulting in a 0.15 mM H<sub>2</sub>SO<sub>4</sub> and 4 mM NaBr solution. Measurements including H<sub>2</sub>O<sub>2</sub> were performed in 0.15 mM H<sub>2</sub>SO<sub>4</sub> + 4 mM NaBr spiked with different amounts of H<sub>2</sub>O<sub>2</sub> dilution to adjust the desired concentration. The H<sub>2</sub>O<sub>2</sub> dilution was obtained from a 30% H<sub>2</sub>O<sub>2</sub> stock solution (Perhydrol, Merck, Germany). For experiments with changing levels of diluted gases, the process media or the outer side of the tubular membrane was flushed with nitrogen or mixtures of nitrogen and O<sub>2</sub> using a gas mixing station with programmable mass flow controllers (IL-GMix41, HiTec Zhang, Germany).

**3.2. Electrochemical Instrumentation.** The fabricated sensor plugs were used in a 3-electrode setup. Two out of the three Pt wire electrodes were used as working and counter electrodes. The Ag/AgBr pseudoreference was used as reference electrode for all chronoamperometric measurements, and all potentials refer to this electrode. All electrochemical measurements were controlled by a potentiostat (Compact-Stat, Ivium Technologies, The Netherlands).

**3.3. Fabrication of the Electrochemical Sensors.** The electrochemical sensor plugs for insertion into the additively manufactured microreactor were fabricated based on a previously described process.<sup>31</sup> The sensor plug consisted of a polymer housing (Loctite Stycast 2057 and Loctite Cat 9, Henkel, Germany) that encloses three Pt wire electrodes with a diameter of 300  $\mu\text{m}$  (99.99%; ChemPUR, Germany) and a silver wire electrode with a diameter of 500  $\mu\text{m}$  (99.99%; ChemPUR, Germany) as shown in Figure 1B. A poly-(hydroxyethyl methacrylate) (pHEMA) membrane on each electrode (Figure 1B) ensured a diffusion-limited mass-transport regime, resulting in a wide linear concentration range. A schematic of the entire reactor concept with the indicated sensor positions can be seen in Figure 1B.

**3.4. Electrochemical Sensor Protocol.** The integrated electrochemical sensors enable the monitoring of the direct synthesis of H<sub>2</sub>O<sub>2</sub> from O<sub>2</sub> and H<sub>2</sub> by online quantification of the concentration of each reactant and the product. The Pt-based sensors allow the simultaneous quantification of H<sub>2</sub>O<sub>2</sub>, H<sub>2</sub>, and O<sub>2</sub>.<sup>29</sup> To evaluate the additively manufactured reactor and its tubular design, quantifications of H<sub>2</sub>O<sub>2</sub> as the liquid product and dissolved O<sub>2</sub> as the gaseous reactant were chosen. The used 3-step chronoamperometric protocol is illustrated in Figure 1C. The first potential of 0.925 V leads to the formation of Pt oxide at the electrode surface as a prerequisite for the

subsequent H<sub>2</sub>O<sub>2</sub> detection by oxidation. The 15 s duration was long enough to completely oxidize the Pt surface and led to a concentration dependent detection current for changing H<sub>2</sub>O<sub>2</sub> concentrations in the process medium. The second step polarizes the electrode negatively to  $-0.4$  V for 10 s. In this step, the Pt oxide gets reduced and leads to a bare Pt surface. At this bare Pt surface, the level of dissolved O<sub>2</sub> is measured by direct electrochemical reduction in the third step at a potential of  $-0.3$  V. Again, the length of the third step at 10 s was long enough to reach a steady state current response.

## 4. RESULTS AND DISCUSSION

**4.1. Additive Manufacturing of the Reactor.** The individual reactor components feed, reaction body, and drain were manufactured by means of the PBF-LB/M process. The CAD model was designed by using Autodesk Inventor. The individual components were fabricated on the described Realizer SLM 125 (DMG Mori, Germany) from stainless steel (1.4404, Carpenter Additive, USA) (Figure 2). Although the build plate and build space theoretically allow multiple components to be fabricated at the same time, the individual components were printed sequentially to avoid surface defects due to the metal slag splashing off. After printing, the support structures required for anchoring the printed part to the build plate were milled off. The sides of the components that later served as sealing surfaces were milled over to remove any unevenness caused by the printing process. The fits, for example, for the subsequent installation of the electrochemical sensors or for chambering the O-rings, were subsequently integrated by milling the specified geometries. Due to the unavoidable overhangs caused by the sensor fits, direct printing of the geometries was not possible. When handling pure O<sub>2</sub>, care must be taken to ensure that components that come into contact with the gas are free of grease, as oil and grease residues that come into contact with O<sub>2</sub> pose a high fire risk.<sup>55</sup> Since all components of the reactor system are in direct contact with pure O<sub>2</sub>, all machining postprocessing steps were performed as dry milling.

**4.2. Sensor Flow Rate Dependency.** Once the assembled reactor was proven to be gastight and no leakage of liquid into the gas compartments was detected, measurements with inserted electrochemical sensors were conducted inside the microreactor's reaction channel. To obtain meaningful concentration measurements of the dissolved gases and H<sub>2</sub>O<sub>2</sub> at the sensor positions, the sensors operate ideally flow rate independent.

The electrodes of the sensor plugs are covered with a hydrogel membrane. This hydrogel membrane acts as a diffusion barrier in order to achieve a diffusion-limited detection regime. Ideally, the concentration gradient at the sensor electrode occurs entirely within the hydrogel if the medium flow provides a constant concentration at the hydrogel surface, and all analytes are converted at the electrode surface at the bottom of the membrane. To measure flow rate dependency, the process medium under ambient conditions presaturated with 256  $\mu\text{M}$  of dissolved O<sub>2</sub> was aspirated through the reactor at different flow rates by adjusting the pumping rate of the peristaltic pump. The gas-side of the membrane was kept under ambient conditions for the entire measurement. This minimizes the O<sub>2</sub> diffusion across the membrane. For each flow rate, 10 measurement cycles were averaged to exclude fluctuations in the measured signal that are not related to the change in flow rate.

The chronoamperometric protocol includes a step for the formation of Pt oxide required for  $\text{H}_2\text{O}_2$  detection (Figure 1C). Figure 3A shows the flow rate dependency of Pt oxide formation. The signal is flow rate independent, as expected, and demonstrates a stable electrochemical cell, constant catalytic activity of the electrode, and a stable electrode/hydrogel system. Figure 3B shows the corresponding dissolved  $\text{O}_2$  measurement, which is also flow rate independent in the range of 0 to  $5.6 \text{ mL min}^{-1}$ . The described measurements were conducted with and without inserted structured catalyst carriers. Both Figure 2A and B contain a comparison of each measured current for the two different setups. Neither for the Pt oxide formation current nor for the  $\text{O}_2$  reduction current shows a different flow rate dependency with a structured catalyst carrier inside the process chamber. This result demonstrates the flow independent measurement of a dissolved reactant gas in the microreactor channel by integrated microsensors, uninfluenced by the integration of the structured catalyst. For all subsequent experiments, flow

rates in the investigated range between 1 and  $5.6 \text{ mL min}^{-1}$  were used.

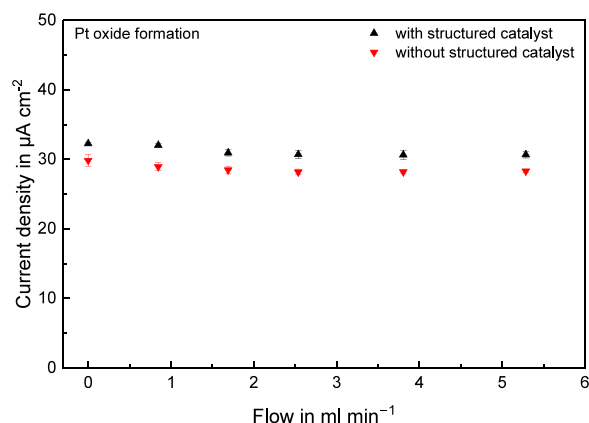
Hereby, we demonstrated that the flow rate within the microreactor can be adjusted in order to control the reaction without compromising the quality of the sensor signals. The electrochemical sensors provide adequate information about the analyte concentrations in the medium flow.

**4.3. Hydrogen Peroxide Monitoring.** A specific use case for flow microreactors is the direct synthesis of  $\text{H}_2\text{O}_2$ . This synthesis reaction can be realized using the microreactor described here (Figure 1A). In order to demonstrate the capability of the electrochemical sensors to detect and quantify  $\text{H}_2\text{O}_2$  inside the acidic process media, calibration measurements were carried out.

For the calibration of  $\text{H}_2\text{O}_2$ , process media under ambient conditions possessing a dissolved  $\text{O}_2$  concentration of roughly  $255 \mu\text{M}$ , with five different concentrations of  $\text{H}_2\text{O}_2$  between 0 and  $2,000 \mu\text{M}$ , were pumped through the microreactor from lowest to highest concentration. In Figure 4A, the time-transient current density is shown, forming a staircase-shaped signal without fluctuations or any drift. The gray boxes in the

### Flowrate dependency inside microreactor

#### A: Flowrate dependency of Pt oxide formation



#### B: Flowrate dependency of $\text{O}_2$ reduction

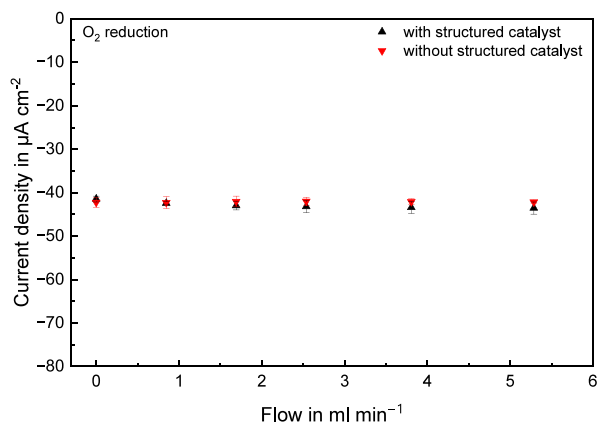
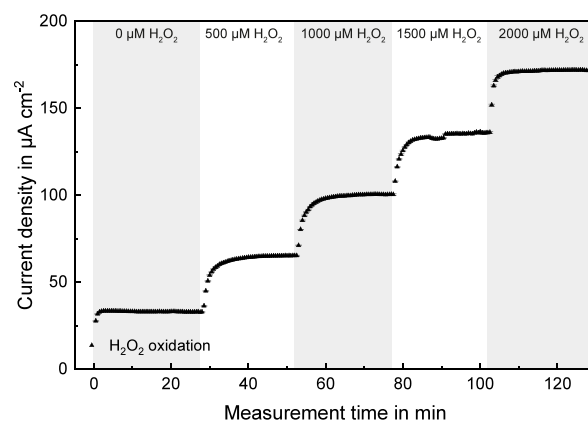


**Figure 3.** Investigation of the sensor's flow rate dependency inside the microreactor. (A) Measured signal of Pt oxide formation for different flow rates with structured catalyst (black triangles) and without structured catalyst (red triangles) placed inside the liquid channel. (B) Measured signal of the  $\text{O}_2$  reduction for different flow rates with structured catalyst (black triangles) and without structured catalyst (red triangles) placed inside the liquid channel.

### On-line $\text{H}_2\text{O}_2$ sensing by oxidation in membrane reactor

#### A: On-line signal of $\text{H}_2\text{O}_2$ oxidation



#### B: $\text{H}_2\text{O}_2$ calibration by oxidation current

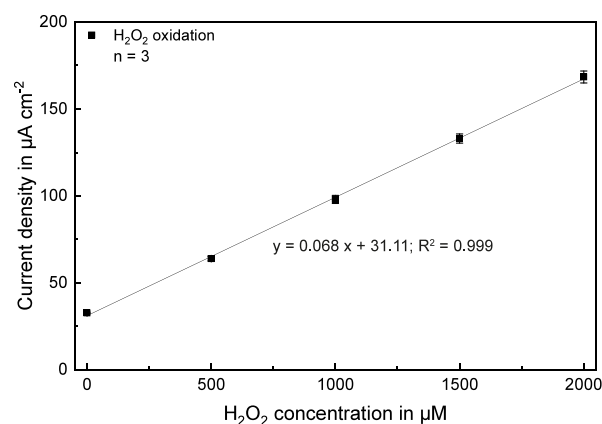


**Figure 4.** Online calibration of hydrogen peroxide inside the microreactor by electrochemical oxidation of hydrogen peroxide in acidic process media. (A) Time transient signal of the measured current response showing the dynamics inside the reactor. (B) Highly linear calibration curve for hydrogen peroxide over a wide range of concentrations with high sensitivity.

plot indicate the point in time at which the electrolyte reservoirs were changed. Therefore, the delay between the edge of a gray-white intersection and the increasing current is caused by the time the process medium needs to flow through the peripheral tubing and the length of the reaction channel to the sensor. The exchange of the media did not lead to a vertical slope, meaning that the sensor is able to monitor the dynamics of the concentration exchange in the flowing process media. The corresponding calibration curve is shown in Figure 4B. Across the entire range from 0 to 2,000  $\mu\text{M}$   $\text{H}_2\text{O}_2$ , the sensor signal was highly linear ( $R^2 = 0.999$ ) and showed a high sensitivity of  $68 \text{ nA cm}^{-2} \mu\text{M}^{-1}$ , demonstrating that the sensor was operated in a diffusion-limited regime. Based on  $3\sigma$  of the blank signal, the detection limit was around  $3.5 \mu\text{M}$ . The offset was caused by background currents from the presence of bromide in the media. Overall, the sensitivity can be adjusted by different membrane thicknesses, according to the desired concentration range.

An additional calibration of  $\text{H}_2\text{O}_2$  was conducted via its reduction at the bare platinum surface under continuous flow for the same range of concentration (Figure 5A). For this calibration, the third potential step of the chronoamperometric protocol was used. The same potential is used for the quantification of dissolved oxygen. The reduction of  $\text{H}_2\text{O}_2$  showed a sensitivity of  $62 \text{ nA cm}^{-2} \mu\text{M}^{-1}$ , which is in very good agreement with the sensitivity for the oxidation. Furthermore, the calibration at the potential that is used for the oxygen reduction shows a linear correlation ( $R^2 = 0.999$ ) between the concentration of  $\text{H}_2\text{O}_2$  and the current response (Figure 5B). Thus, the contribution of the  $\text{H}_2\text{O}_2$  related current to the superposition of currents at the oxygen detection potential can be subtracted by knowing the concentration of  $\text{H}_2\text{O}_2$  by evaluating the current response derived in the previous potential step.

The  $\text{H}_2\text{O}_2$  measurements demonstrated that the micro-sensors integrated in the additively manufactured microreactor enable a sensitive, precise, and reproducible in situ measurement of concentrations in the liquid phase within each module, which can either be a presaturated reactant or product of the reaction.

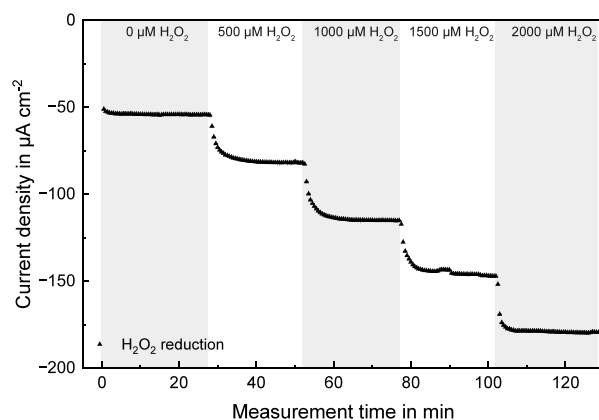
**4.4. Oxygen Monitoring.** Besides  $\text{H}_2\text{O}_2$ , the sensor will be used to detect and quantify dissolved gases in the process medium. In the  $\text{H}_2\text{O}_2$  direct synthesis,  $\text{O}_2$  will be applied to the outer side of the tubular membrane and has to diffuse across that membrane from the gas-phase into the process medium (Figure 1A). This measurement validates the reactor concept.

For these experiments, the process medium was flushed with nitrogen prior to measurement in order to remove any dissolved  $\text{O}_2$ . The process medium was then aspirated through the reaction channel inside the tubular membrane. The gas inlet of the reactor was connected to a gas mixing station, and the outside of the membrane thus flushed with  $450 \text{ mL min}^{-1}$  nitrogen or mixtures of nitrogen and  $\text{O}_2$ . The concentration gradient across the membrane led to the diffusion of  $\text{O}_2$  from the gas phase into the liquid phase. At the end of the reaction chamber, the process medium with its changed content of dissolved  $\text{O}_2$  passes the sensor, and the concentration of dissolved  $\text{O}_2$  can be measured.

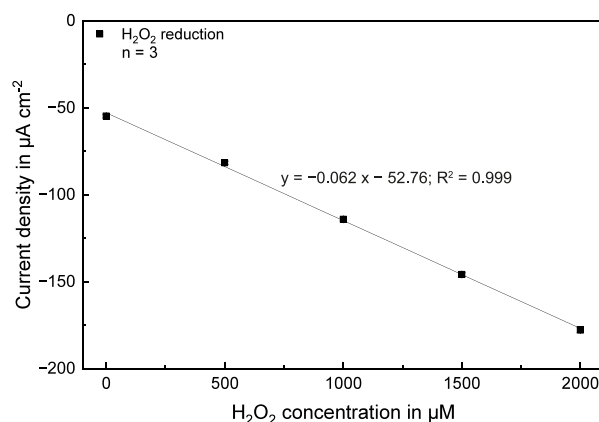
The time transient signal for the detection of dissolved  $\text{O}_2$  is displayed in Figure 6A. At the beginning of the measurement, both the process medium and the outer side of the membrane are flushed with pure nitrogen. Hence, there is no dissolved  $\text{O}_2$  in the process medium, and the sensor shows a very low signal

## On-line $\text{H}_2\text{O}_2$ sensing by reduction in membrane reactor

### A: On-line signal of $\text{H}_2\text{O}_2$ reduction



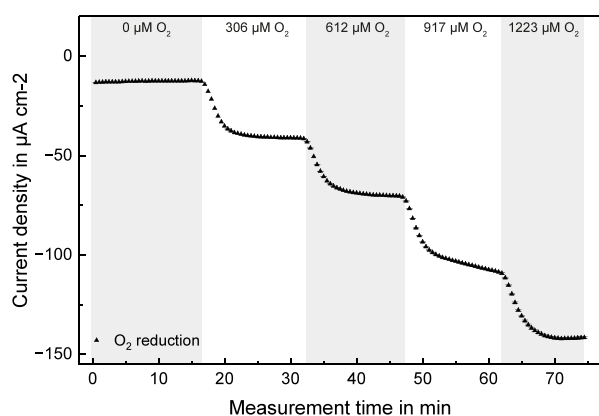
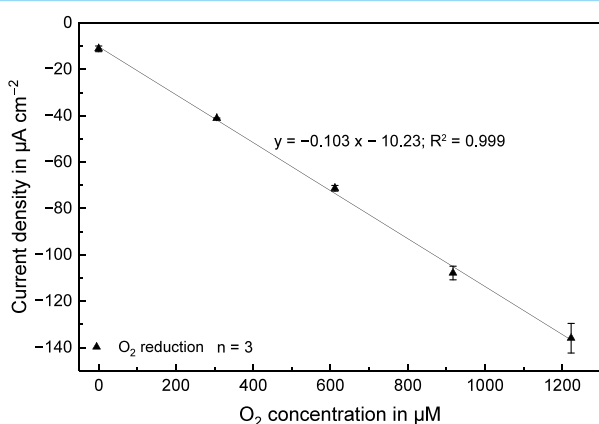
### B: $\text{H}_2\text{O}_2$ calibration by reduction current



**Figure 5.** Online calibration of hydrogen peroxide in the presence of oxygen inside the microreactor by electrochemical reduction of hydrogen peroxide in acidic process media. (A) Time transient signal of the measured current response showing the dynamics inside the reactor. (B) Highly linear calibration curve for hydrogen peroxide in the presence of oxygen over a wide range of concentrations with high sensitivity.

with a slight offset from 0. The remaining reduction current is attributed to the nonspecific background from the presence of bromide. After 15 min, the outside of the membrane was flushed with  $450 \text{ mL min}^{-1}$  of a gas mixture consisting of 75%  $\text{N}_2$  and 25%  $\text{O}_2$  resulting in  $306 \mu\text{M}$  dissolved  $\text{O}_2$  in the process medium. In equal steps of 15 min each, the  $\text{O}_2$  volume fraction of the gas mixture was increased to 50, 75, and 100% leading to dissolved concentrations of 612, 917, and  $1223 \mu\text{M}$ . The dynamics of the dissolved gas concentrations can be observed in situ and in real time (Figure 6A), providing valuable information about the  $\text{O}_2$  concentration inside the reaction channel, which is not accessible with traditional measurement methods. The resulting calibration curve for the used setup displayed in Figure 6 shows a high linearity with a  $R^2$  of 0.999 and a high sensitivity of  $103 \text{ nA cm}^{-2} \mu\text{M}^{-1}$  across the entire concentration range from 0 to 1 bar of the  $\text{O}_2$  partial pressure.

The dissolved  $\text{O}_2$  measurements demonstrated that the integrated sensors allow the quantification of gases entering the microreactor through the tubular membrane and dissolving in the liquid phase. Consequently, they enable the monitoring of

Calibration of dissolved O<sub>2</sub> in membrane reactorA: On-line signal of dissolved O<sub>2</sub> calibrationB: Dissolved O<sub>2</sub> calibration

**Figure 6.** Online calibration of dissolved oxygen in the reactor's liquid phase by gas dosing through the membrane. (A) O<sub>2</sub> reduction current. (B) Calibration curve for dissolved O<sub>2</sub> with high linearity and high sensitivity.

the saturation after each reaction body module, which is required for controlling the process.

**4.5. In Situ Monitoring of Sensor Performance and Stability.** An important factor for continuous online measurements in process engineering is the long-term stability and lifetime of the sensors, especially for harsh environments, such as acidic media and the presence of halide ions. To investigate different aspects of sensor stability, two types of measurements were conducted. First, we performed long-term continuous measurements in process medium under ambient conditions with a sensor protocol in the time scale of the measurement protocol for a total duration of up to 1 week. Second, we investigated intensified aging of the electrodes in the process medium with and without bromide in order to mimic even longer durations. In addition to the standard measurements protocol (Figure 1C), a first potential step at 1 V for 5 s was added to better track the influence of the presence of bromide. Furthermore, we explored the investigation of this background to process the measurement signal in order to further increase signal stability by correcting the analyte unspecific fluctuations.

**4.5.1. Long-Term Continuous Measurements.** To demonstrate the continuous use in process monitoring, we performed long-term measurements, using the extended measurement protocol over up to 1 week. After conditioning the electrode's

surface, the entire chronoamperometric protocol was applied continuously over 7 days and more than 19,000 measurement cycles. After each block of 1,000 measurement cycles, one cycle was evaluated, regarding the currents for Pt oxide formation and electrochemical reduction of O<sub>2</sub>. All of the analyzed data points were normalized to the initial value to highlight changes in the measured signals.

Cyclic voltammetry was conducted in diluted sulfuric acid and in diluted sulfuric acid with added sodium bromide in order to correlate the surface chemistry of the platinum electrode inside the process medium with the current response of the chronoamperometric protocol (Figure 7A). The cyclic voltammogram conducted in the presence of sodium bromide shows a prominent, additional oxidation peak for potentials higher than 850 mV vs Ag/AgCl. The location of the bromide oxidation is superimposed with the oxidation of the electrode's platinum surface and the oxidation of H<sub>2</sub>O<sub>2</sub>.<sup>31</sup> The resulting signals are shown in Figure 7B along the measurement time in days. The O<sub>2</sub> reduction current (black curve), which is less affected by the background signal of bromide, showed a very small variation over the entire 7 day measurement period. The dashed lines in the graph indicate the marks of  $\pm 5\%$  with respect to the initial value. For all times, the measured O<sub>2</sub> reduction signal was within that margin.

The current at the H<sub>2</sub>O<sub>2</sub> detection potential (0.95 V, red curve) was more affected than the O<sub>2</sub> reduction current by the fluctuations of the background signal because it is affected by Pt oxide formation and measured at a potential at which the bromide oxidation already sets in. Therefore, the directly measured current at this potential exceeded the tolerance of  $\pm 5\%$  (Figure 7B). The 1 V potential step added prior to 0.95 V was then used to correct the effect of the background. Therefore, we recalculated the current at 0.95 V based on the fluctuations of the current at 1 V by weighted correction to account for electrode status during analyte detection. The resulting signal for the Pt oxide formation at 0.95 V (blue curve) was within the 5% margin for the entire measurement period (Figure 7B).

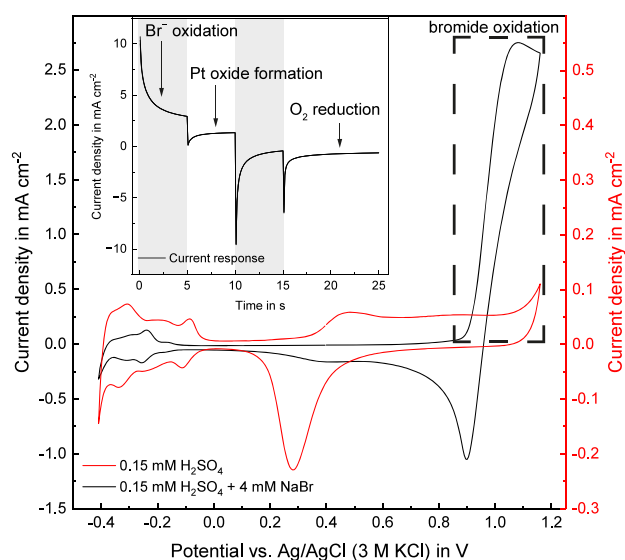
These results demonstrated that the electrochemical sensors are capable of quantifying O<sub>2</sub> over a full week continuously without any drift or major fluctuations in the acidic process medium (pH 3.5). Since the Pt oxide formation current is a good marker for the state of the electrode,<sup>56,57</sup> we conclude that the electrode does not degrade over this time. In addition, the multistep chronoamperometric protocol was used to correct unspecific background from the presence of bromide and improve the signal stability, toward more robust and self-calibrating sensors in harsh environments.

**4.5.2. Intensified Aging and Electrode Lifetime.** An investigation of intensified aging with a shorter measurement protocol was conducted. The intensified aging was achieved by switching rapidly between 1 V (Pt oxide formation) and  $-0.3$  V (O<sub>2</sub> reduction) for 100 ms each.<sup>57</sup> Since Pt electrodes inevitably undergo dissolution under cyclic load, especially in acidic media,<sup>57,58</sup> this method artificially accelerated electrode degradation and allows estimations about total sensor lifetime.

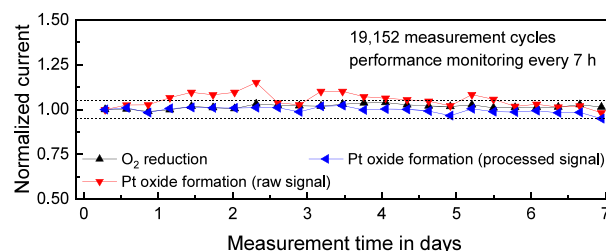
The comparison of the sensor performance under intensified aging in 0.15 M H<sub>2</sub>SO<sub>4</sub> (pH 3.5) with and without bromide can be seen in Figure 7C. The measured currents of Pt oxide formation and O<sub>2</sub> reduction were normalized to the initial value in each electrolyte in order to compare the changes in the electrodes surface, catalytic activity, and O<sub>2</sub> detection of the sensor.

## Sensor performance monitoring

## A: Influence of bromide oxidation



## B: Continuous long-term measurement



## C: Electrode stability under intensified aging

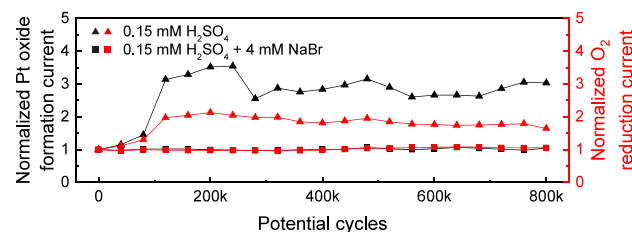


**Figure 7.** Sensor performance monitoring for continuous measurement and intensified aging in acidic (pH = 3.5) media. (A) Comparison of cyclic voltammograms conducted in 0.15 mM  $\text{H}_2\text{SO}_4$  (red curve) and 0.15 mM  $\text{H}_2\text{SO}_4$  + 4 mM NaBr (black curve); measured current of the chronoamperometric protocol with a description of the electrochemical processes as inset. (B) Sensor performance monitoring via quantification of Pt oxide formation and  $\text{O}_2$  sensing along 7 day continuous measurement, including processed signal for improved stability. (C) Investigation of the electrode stability under intensified aging. Data points show performance evaluation during 800,000 cycles of accelerated aging. In the presence of bromide, Pt oxide formation and the  $\text{O}_2$  sensor signal are stable.

The Pt oxide formation current increases by nearly a factor of 4 over the first 280,000 potential cycles in diluted sulfuric acid without bromide before it fluctuates around an average value of nearly 3 times the initial current. The increase of Pt oxide formation current is known to happen when potential-controlled degradation is performed on Pt in acidic media.<sup>57</sup> The effect can be attributed to roughening of the surface due to Pt dissolution and the subsequent increase in the accessible surface. While a roughening typically is not expected to influence the  $\text{O}_2$  signal, an increase was also observed for the  $\text{O}_2$  signal but to a lesser degree (Figure 7C).

Interestingly, with added sodium bromide, no current increase at all can be seen in diluted sulfuric acid, even though the pH remains at 3.5. Both the Pt oxide formation current and the  $\text{O}_2$  reduction current stay at their initial values (Figure 7C). Knowing that bromide inhibits the formation of Pt oxide, which can be seen in studies applying cyclic voltammograms,<sup>31</sup> we conclude that the inhibited formation of Pt oxide prevents the known degradation mechanism of Pt. Evaluating our measurements, we conclude that the added bromide has a protective nature with regard to the Pt degradation in acidic media.

Overall, cyclic load, such as in chronoamperometry, leads to Pt dissolution and roughening of the surface in acidic media over hundreds of thousands of cycles, generally limiting sensor stability. However, in relation to the standard protocol shown in Figure 7B, 100,000 cycles represent a continuous measurement over several weeks. In the case of the presence of bromide, even prolonged cycling does not lead to a performance decrease over up to 800,000 cycles, which corresponds to an estimated use of almost a year. In addition, we have shown that by tracking Pt oxide formation as an

indicator for the electrode state, changes in sensor stability can be detected online and even corrected.

## 5. CONCLUSIONS

We developed a microsensors equipped concept of an additively manufacturable, tubular stainless steel microreactor for the direct synthesis of  $\text{H}_2\text{O}_2$  on a noble metal catalyst. Under consideration of the given requirements by the fabrication method, the desired chemical reaction, and the necessary process conditions, the microreactor was fabricated in a modular approach using metal 3D printing by PBF-LB/M. The fabricated parts of feed, reaction body, and drain were assembled in combination with a tubular, ceramic membrane coated with PDMS and the structured catalyst. The assembled setup, together with integrated microsensors, was successfully tested for water- and gas-tightness.

Miniaturized, electrochemical sensors featuring Pt electrodes were successfully integrated in the additively manufactured reactor and allowed continuous, online measurement inside the microreactor's reaction chamber.  $\text{H}_2\text{O}_2$  concentration was measured continuously directly within the process medium with high linearity and sensitivity. Access to time transient concentrations in the tube-in-tube design delivers important insights into the dynamics of the process, highlighting the power of electrochemical sensors applied in process engineering. Such in situ real-time detection is hard to achieve by other methods.

The concept of the membrane microreactor, with a tubular membrane separating the liquid process media from the outer gas-phase, was confirmed by measurements of dissolved  $\text{O}_2$  after its membrane passage in the process media. The uninterrupted measurement of dissolved gas concentrations shows the bubble free dosage of gases into the process medium

and enables optimization of processes by resaturating reactants while the process is running.

As sensor stability under harsh conditions is essential for successful process monitoring, we investigated the electrode degradation by the application of the actual measurement protocol. In addition to continuous, stable measurement for a full week, we demonstrated that information gained during the early steps of the advanced chronoamperometric protocol can be used to correct the concentration measurements from background fluctuations to increase the stability. This signal processing within the electrochemical sensor protocol is a crucial step toward more robust and self-calibrating sensors for industrial applications. On top of that, we investigated sensor lifetime using an intensified aging protocol, together with sensor performance characterization, to address electrode stability in acidic and halide ion containing media. In the presence of bromide in the process medium, we estimated a sensor lifetime of nearly one year. This shows that electrochemical methods allow an uninterrupted combination of analyte concentration measurements and electrode degradation monitoring.

In summary, our results emphasize the power of additively manufactured stainless steel microreactors in combination with electrochemical sensors for monitoring and controlling reactions in flow-chemistry. Combining the advantages of stainless steel as a robust material with the possibility to fulfill complex geometric requirements of microreactors by additive manufacturing together with the capability of in situ monitoring inside the reaction channel by electrochemical sensors, we contribute to the next generation of microreactors. Enabling safer, more sustainable, and adjustable processes in a decentralized production, sensor-equipped, 3D-printed microreactors can be a supporting pillar of the paradigm change in the chemical industry toward green chemistry.

## AUTHOR INFORMATION

### Corresponding Author

**Andreas Weltin** – Laboratory for Sensors, IMTEK – Department of Microsystems Engineering and Laboratory for Electrical Instrumentation and Embedded Systems, IMTEK – Department of Microsystems Engineering, University of Freiburg, 79110 Freiburg, Germany; [orcid.org/0000-0001-8288-8266](https://orcid.org/0000-0001-8288-8266); Phone: +49 761 203-7263; Email: [weltin@imtek.de](mailto:weltin@imtek.de)

### Authors

**Moritz Doering** – Laboratory for Sensors, IMTEK – Department of Microsystems Engineering and Laboratory for Electrical Instrumentation and Embedded Systems, IMTEK – Department of Microsystems Engineering, University of Freiburg, 79110 Freiburg, Germany

**Laura L. Trinkies** – Institute of Micro Process Engineering (IMVT), Karlsruhe Institute of Technology, 76344 Eggenstein-Leopoldshafen, Germany

**Jochen Kieninger** – Laboratory for Sensors, IMTEK – Department of Microsystems Engineering and Laboratory for Electrical Instrumentation and Embedded Systems, IMTEK – Department of Microsystems Engineering, University of Freiburg, 79110 Freiburg, Germany; [orcid.org/0000-0001-8220-8814](https://orcid.org/0000-0001-8220-8814)

**Manfred Kraut** – Institute of Micro Process Engineering (IMVT), Karlsruhe Institute of Technology, 76344 Eggenstein-Leopoldshafen, Germany

**Stefan J. Rupitsch** – Laboratory for Electrical Instrumentation and Embedded Systems, IMTEK – Department of Microsystems Engineering, University of Freiburg, 79110 Freiburg, Germany

**Roland Dittmeyer** – Institute of Micro Process Engineering (IMVT), Karlsruhe Institute of Technology, 76344 Eggenstein-Leopoldshafen, Germany; [orcid.org/0000-0002-3110-6989](https://orcid.org/0000-0002-3110-6989)

**Gerald A. Urban** – Laboratory for Sensors, IMTEK – Department of Microsystems Engineering, University of Freiburg, 79110 Freiburg, Germany

Complete contact information is available at: <https://pubs.acs.org/10.1021/acsomega.4c02210>

## Notes

The authors declare no competing financial interest.

## ACKNOWLEDGMENTS

We thank the group for Additive Manufacturing at IMVT under Prof. Christoph Klahn, with special thanks to Manuel Hofheinz, Fabian Rupp, Fabian Grinschek und David Metzger for the manufacturing and postprocessing of the parts. We thank Cornelia Schorle for the conduction of the He-leakage tests. Funding by Deutsche Forschungsgemeinschaft (DFG, German Research Foundation) within Research Unit “ProMiSe” (FOR 2383), project number 274353615, is gratefully acknowledged. We acknowledge support by the Open Access Publication Fund of the University of Freiburg.

## REFERENCES

- (1) Monbaliu, J.-C. M.; Legros, J. Will the next Generation of Chemical Plants Be in Miniaturized Flow Reactors? *Lab Chip* **2023**, *23* (5), 1349–1357.
- (2) Gutmann, B.; Cantillo, D.; Kappe, C. O. Continuous-Flow Technology - A Tool for the Safe Manufacturing of Active Pharmaceutical Ingredients. *Angew. Chemie - Int. Ed.* **2015**, *54* (23), 6688–6728.
- (3) Movsisyan, M.; Delbeke, E. I. P.; Berton, J. K. E. T.; Battilocchio, C.; Ley, S. V.; Stevens, C. V. Taming Hazardous Chemistry by Continuous Flow Technology. *Chem. Soc. Rev.* **2016**, *45* (18), 4892–4928.
- (4) Pennemann, H.; Kolb, G. Review: Microstructured Reactors as Efficient Tool for the Operation of Selective Oxidation Reactions. *Catal. Today* **2016**, *278*, 3–21.
- (5) Voloshin, Y.; Lawal, A. Overall Kinetics of Hydrogen Peroxide Formation by Direct Combination of H<sub>2</sub> and O<sub>2</sub> in a Microreactor. *Chem. Eng. Sci.* **2010**, *65* (2), 1028–1036.
- (6) Wang, N.; Ma, S.; Zuo, P.; Duan, J.; Hou, B. Recent Progress of Electrochemical Production of Hydrogen Peroxide by Two-Electron Oxygen Reduction Reaction. *Adv. Sci.* **2021**, *8* (15), 2100076.
- (7) Filippi, J.; Miller, H. A.; Nasi, L.; Pagliaro, M. V.; Marchionni, A.; Melchionna, M.; Fornasiero, P.; Vizza, F. Optimization of H<sub>2</sub>O<sub>2</sub> Production in a Small-Scale off-Grid Buffer Layer Flow Cell Equipped with Cobalt@N-Doped Graphitic Carbon Core–Shell Nanohybrid Electrocatalyst. *Mater. Today Energy* **2022**, *29*, 101092.
- (8) Zhang, Y.; Mascaretti, L.; Melchionna, M.; Henrotte, O.; Kment, S.; Fornasiero, P.; Naldoni, A. Thermoplasmonic In Situ Fabrication of Nanohybrid Electrocatalysts over Gas Diffusion Electrodes for Enhanced H<sub>2</sub>O<sub>2</sub> Electrosynthesis. *ACS Catal.* **2023**, *13* (15), 10205–10216.
- (9) Capel, A. J.; Edmondson, S.; Christie, S. D. R.; Goodridge, R. D.; Bibb, R. J.; Thurstans, M. Design and Additive Manufacture for Flow Chemistry. *Lab Chip* **2013**, *13* (23), 4583–4590.
- (10) Blakey-Milner, B.; Gradl, P.; Snedden, G.; Brooks, M.; Pitot, J.; Lopez, E.; Leary, M.; Berto, F.; du Plessis, A. Metal Additive

- Manufacturing in Aerospace: A Review. *Mater. Des.* **2021**, *209*, 110008.
- (11) Jiménez, A.; Bidare, P.; Hassanin, H.; Tarlochan, F.; Dimov, S.; Essa, K. Powder-Based Laser Hybrid Additive Manufacturing of Metals: A Review. *Int. J. Adv. Manuf. Technol.* **2021**, *114* (1–2), 63–96.
- (12) Lewandowski, J. J.; Seifi, M. Metal Additive Manufacturing: A Review of Mechanical Properties. *Annu. Rev. Mater. Res.* **2016**, *46*, 151–186.
- (13) Moeinfar, K.; Khodabakhshi, F.; Kashani-bozorg, S. F.; Mohammadi, M.; Gerlich, A. P. A Review on Metallurgical Aspects of Laser Additive Manufacturing (LAM): Stainless Steels, Nickel Superalloys, and Titanium Alloys. *J. Mater. Res. Technol.* **2022**, *16*, 1029–1068.
- (14) Stetter, J. R.; Penrose, W. R.; Yao, S. Sensors, Chemical Sensors, Electrochemical Sensors, and ECS. *J. Electrochem. Soc.* **2003**, *150* (2), S11.
- (15) Privett, B. J.; Shin, J. H.; Schoenfish, M. H. Electrochemical Sensors. *Anal. Chem.* **2008**, *80* (12), 4499–4517.
- (16) Lenarda, A.; Bakandritsos, A.; Bevilacqua, M.; Tavagnacco, C.; Melchionna, M.; Naldoni, A.; Steklý, T.; Otyepka, M.; Zbořil, R.; Fornasiero, P. Selective Functionalization Blended with Scaffold Conductivity in Graphene Acid Promotes H<sub>2</sub>O<sub>2</sub> Electrochemical Sensing. *ACS Omega* **2019**, *4* (22), 19944–19952.
- (17) Wang, X. D.; Wolfbeis, O. S. Fiber-Optic Chemical Sensors and Biosensors (2015–2019). *Anal. Chem.* **2020**, *92* (1), 397–430.
- (18) Li, J.; Simek, H.; Ilioaie, D.; Jung, N.; Bräse, S.; Zappe, H.; Dittmeyer, R.; Ladewig, B. P. In Situ Sensors for Flow Reactors-A Review. *React. Chem. Eng.* **2021**, *6* (9), 1497–1507.
- (19) Chen, W.; Cai, S.; Ren, Q. Q.; Wen, W.; Zhao, Y. Di. Recent Advances in Electrochemical Sensing for Hydrogen Peroxide: A Review. *Analyst* **2012**, *137* (1), 49–58.
- (20) Tsaplev, Y. B. Chemiluminescence Determination of Hydrogen Peroxide. *J. Anal. Chem.* **2012**, *67* (6), 506–514.
- (21) Hu, Y.; Zhang, Z.; Yang, C. The Determination of Hydrogen Peroxide Generated from Cigarette Smoke with an Ultrasensitive and Highly Selective Chemiluminescence Method. *Anal. Chim. Acta* **2007**, *601* (1), 95–100.
- (22) Hu, A. L.; Liu, Y. H.; Deng, H. H.; Hong, G. L.; Liu, A. L.; Lin, X. H.; Xia, X. H.; Chen, W. Fluorescent Hydrogen Peroxide Sensor Based on Cupric Oxide Nanoparticles and Its Application for Glucose and L-Lactate Detection. *Biosens. Bioelectron.* **2014**, *61*, 374–378.
- (23) Khorami, H. A.; Botero-Cadavid, J. F.; Wild, P.; Djilali, N. Spectroscopic Detection of Hydrogen Peroxide with an Optical Fiber Probe Using Chemically Deposited Prussian Blue. *Electrochim. Acta* **2014**, *115*, 416–424.
- (24) Maier, M. C.; Lebl, R.; Sulzer, P.; Lechner, J.; Mayr, T.; Zadavec, M.; Slama, E.; Pfanner, S.; Schmolzer, C.; Pöchlauer, P.; Kappe, C. O.; Gruber-Woelfler, H. Development of Customized 3D Printed Stainless Steel Reactors with Inline Oxygen Sensors for Aerobic Oxidation of Grignard Reagents in Continuous Flow. *React. Chem. Eng.* **2019**, *4* (2), 393–401.
- (25) Tjell, A.; Jud, B.; Schaller-Ammann, R.; Mayr, T. Optical Hydrogen Peroxide Sensor for Measurements in Flow. *Sensors Actuators B Chem.* **2024**, *400*, 134904.
- (26) Inoue, T.; Ohtaki, K.; Murakami, S.; Matsumoto, S. Direct Synthesis of Hydrogen Peroxide Based on Microreactor Technology. *Fuel Process. Technol.* **2013**, *108*, 8–11.
- (27) Menegazzo, F.; Manzoli, M.; Signoretto, M.; Pinna, F.; Strukul, G. H<sub>2</sub>O<sub>2</sub> Direct Synthesis under Mild Conditions on Pd-Au Samples: Effect of the Morphology and of the Composition of the Metallic Phase. *Catal. Today* **2015**, *248*, 18–27.
- (28) Shi, X.; Back, S.; Gill, T. M.; Siahrostami, S.; Zheng, X. Electrochemical Synthesis of H<sub>2</sub>O<sub>2</sub> by Two-Electron Water Oxidation Reaction. *Chem.* **2021**, *7* (1), 38–63.
- (29) Urban, S.; Deschner, B. J.; Trinkies, L. L.; Kieninger, J.; Kraut, M.; Dittmeyer, R.; Urban, G. A.; Weltin, A. In Situ Mapping of H<sub>2</sub>, O<sub>2</sub>, and H<sub>2</sub>O<sub>2</sub> in Microreactors: A Parallel, Selective Multianalyte Detection Method. *ACS Sensors* **2021**, *6* (4), 1583–1594.
- (30) Selinsek, M.; Kraut, M.; Dittmeyer, R. Experimental Evaluation of a Membrane Micro Channel Reactor for Liquid Phase Direct Synthesis of Hydrogen Peroxide in Continuous Flow Using Nafion Membranes for Safe Utilization of Undiluted Reactants. *Catalysts* **2018**, *8* (11), 556.
- (31) Urban, S.; Weltin, A.; Flamm, H.; Kieninger, J.; Deschner, B. J.; Kraut, M.; Dittmeyer, R.; Urban, G. A. Electrochemical Multisensor System for Monitoring Hydrogen Peroxide, Hydrogen and Oxygen in Direct Synthesis Microreactors. *Sensors Actuators, B Chem.* **2018**, *273*, 973–982.
- (32) Selinsek, M.; Bohrer, M.; Vankayala, B. K.; Haas-Santo, K.; Kraut, M.; Dittmeyer, R. Towards a New Membrane Micro Reactor System for Direct Synthesis of Hydrogen Peroxide. *Catal. Today* **2016**, *268*, 85–94.
- (33) Klahn, C.; Meboldt, M.; Fontana, F.; Leutenecker-Twelsiek, B.; Jansen, J. *Entwicklung Und Konstruktion Für Die Additive Fertigung: Grundlagen Und Methoden Für den Einsatz in Industriellen Endkundenprodukten*, 1st ed.; Vogel Business Media, 2018.
- (34) Atzeni, E.; Salmi, A. Economics of Additive Manufacturing for End-Usable Metal Parts. *Int. J. Adv. Manuf. Technol.* **2012**, *62* (9–12), 1147–1155.
- (35) Schneck, M.; Gollnau, M.; Lutter-Günther, M.; Haller, B.; Schlick, G.; Lakomic, M.; Reinhart, G. Evaluating the Use of Additive Manufacturing in Industry Applications. *Proc. CIRP* **2019**, *81*, 19–23.
- (36) Charles, A.; Elkaseer, A.; Paggi, U.; Thijs, L.; Hagenmeyer, V.; Scholz, S. Down-Facing Surfaces in Laser Powder Bed Fusion of Ti6Al4V: Effect of Dross Formation on Dimensional Accuracy and Surface Texture. *Addit. Manuf.* **2021**, *46*, 102148.
- (37) Zeng, K. Optimization of Support Structures for Selective Laser Melting. PhD thesis, University of Louisville: Louisville, USA, 2015.
- (38) Calignano, F. Design Optimization of Supports for Overhanging Structures in Aluminum and Titanium Alloys by Selective Laser Melting. *Mater. Des.* **2014**, *64*, 203–213.
- (39) Grinschek, F.; Charles, A.; Elkaseer, A.; Klahn, C.; Scholz, S. G.; Dittmeyer, R. Gas-Tight Means Zero Defects - Design Considerations for Thin-Walled Fluidic Devices with Overhangs by Laser Powder Bed Fusion. *Mater. Des.* **2022**, *223*, 111174.
- (40) Li, Z.; Xu, R.; Zhang, Z.; Kucukkoc, I. The Influence of Scan Length on Fabricating Thin-Walled Components in Selective Laser Melting. *Int. J. Mach. Tools Manuf.* **2018**, *126*, 1–12.
- (41) Chen, C.; Xiao, Z.; Zhu, H.; Zeng, X. Deformation and Control Method of Thin-Walled Part during Laser Powder Bed Fusion of Ti6Al4V Alloy. *Int. J. Adv. Manuf. Technol.* **2020**, *110* (11–12), 3467–3478.
- (42) Deutsches Institut für Normung. *Additive Manufacturing - Design - Part 1: Laser-Based Powder Bed Fusion of Metals*; Berlin, 2019.
- (43) Wegner, J.; Ceylan, S.; Kirschning, A. Ten Key Issues in Modern Flow Chemistry. *Chem. Commun.* **2011**, *47* (16), 4583–4592.
- (44) Hansjosten, E.; Wenka, A.; Hensel, A.; Benzinger, W.; Klumpp, M.; Dittmeyer, R. Custom-Designed 3D-Printed Metallic Fluid Guiding Elements for Enhanced Heat Transfer at Low Pressure Drop. *Chem. Eng. Process. - Process Intensif.* **2018**, *130* (May), 119–126.
- (45) Trinkies, L. L.; Ng, D.; Xie, Z.; Hornung, C. H.; Kraut, M.; Dittmeyer, R. Direct Synthesis of Hydrogen Peroxide at Additively Manufactured Fluid Guiding Elements as Structured Catalysts. *Chem. Eng. Process. - Process Intensif.* **2023**, *188*, 109353.
- (46) Trinkies, L. L.; Crone, M.; Türk, M.; Kraut, M.; Dittmeyer, R. Supercritical Deposition of Mono- and Bimetallic Pd and Pt on TiO<sub>2</sub> Additively Manufactured Substrates for the Application in the Direct Synthesis of Hydrogen Peroxide. *Chem. Eng. Process. - Process Intensif.* **2024**, *195*, 109618.
- (47) Hamel, C.; Seidel-Morgenstern, A. Potenzial von Membranen Zur Verbesserten Reaktionsführung von Selektivoxidationen: Katalysator-, Reaktor- Und Prozessebene. *Chemie Ing. Technol.* **2022**, *94* (1–2), 56–69.

- (48) Giacobbe, F. W. Oxygen Permeability of Teflon—PFA Tubing. *J. Appl. Polym. Sci.* **1990**, *39* (5), 1121–1132.
- (49) O'Brien, M.; Baxendale, I. R.; Ley, S. V. Flow Ozonolysis Using a Semipermeable Teflon AF-2400 Membrane To Effect Gas—Liquid Contact. *Org. Lett.* **2010**, *12* (7), 1596–1598.
- (50) Brzozowski, M.; O'Brien, M.; Ley, S. V.; Polyzos, A. Flow Chemistry: Intelligent Processing of Gas—Liquid Transformations Using a Tube-in-Tube Reactor. *Acc. Chem. Res.* **2015**, *48* (2), 349–362.
- (51) Caro, J.; Caspary, K. J.; Hamel, C.; Hoting, B.; Kölsch, P.; Langanke, B.; Nassauer, K.; Schiestel, T.; Schmidt, A.; Schomäcker, R.; Seidel-Morgenstern, A.; Tsotsas, E.; Voigt, I.; Wang, H.; Warsitz, R.; Werth, S.; Wolf, A. Catalytic Membrane Reactors for Partial Oxidation Using Perovskite Hollow Fiber Membranes and for Partial Hydrogenation Using a Catalytic Membrane Contactor. *Ind. Eng. Chem. Res.* **2007**, *46* (8), 2286–2294.
- (52) Liebner, C.; Hieronymus, H.; Heinrich, S.; Edeling, F.; Lange, T.; Klemm, E. *Zündung, Ausbreitung und Unterdrückung in einem Mikroreaktor*. PTB-OAR, 2018.
- (53) Otaola, F.; Mottelet, S.; Guénin, E.; Luart, D.; Leturia, M. Additive Manufacturing of Microstructured Reactors for Organometallic Catalytic Reactions. *Lab Chip* **2023**, 23702.
- (54) Deguchi, T.; Iwamoto, M. Catalytic Properties of Surface Sites on Pd Clusters for Direct H<sub>2</sub>O<sub>2</sub> Synthesis from H<sub>2</sub> and O<sub>2</sub>: A DFT Study. *J. Phys. Chem. C* **2013**, *117* (36), 18540–18548.
- (55) European Industrial Gases Association. *Fire Hazards of Oxygen and Oxygen Enriched Atmospheres*. EIGA, 2018.
- (56) Weltin, A.; Ganatra, D.; König, K.; Joseph, K.; Hofmann, U. G.; Urban, G. A.; Kieninger, J. New Life for Old Wires: Electrochemical Sensor Method for Neural Implants. *J. Neural Eng.* **2020**, *17* (1), 016007.
- (57) Doering, M.; Kieninger, J.; Urban, G. A.; Weltin, A. Electrochemical Microelectrode Degradation Monitoring: In Situ Investigation of Platinum Corrosion at Neutral pH. *J. Neural Eng.* **2022**, *19*, 016005.
- (58) Topalov, A. A.; Cherevko, S.; Zeradjanin, A. R.; Meier, J. C.; Katsounaros, I.; Mayrhofer, K. J. J. Towards a Comprehensive Understanding of Platinum Dissolution in Acidic Media. *Chem. Sci.* **2014**, *5* (2), 631–638.